


Article

The Effect of TIG Welding Heat Input on the Deformation of a Thin Bending Plate and Its Weld Zone

Nan Guo ¹, Hao Hu ¹, Xiaojie Tang ^{2,*}, Xiqiang Ma ^{1,3}  and Xiao Wang ¹

¹ School of Mechatronics Engineering, Henan University of Science and Technology, Luoyang 471003, China; guonan1860@163.com (N.G.); clearlake8@163.com (H.H.); maxiqiang@haust.edu.cn (X.M.); wangxiao@haust.edu.cn (X.W.)

² School of Computer Science, Heze University, Heze 274015, China

³ Longmen Laboratory, Luoyang 471003, China

* Correspondence: tang1xiao@163.com

Abstract: Heat input is a crucial parameter in the process of welding thin plates. It has a direct impact on the quality of the weld and the degree of deformation caused during welding. This study investigates the impact of heat input on the deformation of a thin bending plate and its weld zone using the thermoelastic–plastic finite element method. The accuracy of the model is ascertained using the non-contact inspection method utilizing digital image correlation technology. The welding deformation patterns of thin bending plates with a radius of 500 mm were analyzed at various welding heat inputs ranging from 173 J/mm to 435 J/mm. The results indicate that the finite element prediction model proposed in this paper is highly accurate. It has been observed that, under this range of thermal input, the thin bent plates undergo saddle deformation. By examining the correlation between heat input and the maximum deformation outside of the plane, it has been determined that a heat input of at least 50 J/mm is required for the thin bending plate to experience out-of-plane deformation. Additionally, as the level of heat input increases, so too does the out-of-plane deformation of the thin bending plate. After the completion of the welding cooling process, the transverse shrinkage at the weld seam of the thin bend plate is twice that of the longitudinal shrinkage. However, the transverse deformation of the bend plate is not significantly different from the longitudinal deformation.

Keywords: heat input; thin bent plate; welding; thermo-elasticity



Citation: Guo, N.; Hu, H.; Tang, X.; Ma, X.; Wang, X. The Effect of TIG Welding Heat Input on the Deformation of a Thin Bending Plate and Its Weld Zone. *Coatings* **2023**, *13*, 2008. <https://doi.org/10.3390/coatings13122008>

Academic Editor: Andrew J. Pinkerton

Received: 23 October 2023

Revised: 15 November 2023

Accepted: 23 November 2023

Published: 27 November 2023



Copyright: © 2023 by the authors. Licensee MDPI, Basel, Switzerland. This article is an open access article distributed under the terms and conditions of the Creative Commons Attribution (CC BY) license (<https://creativecommons.org/licenses/by/4.0/>).

1. Introductory

Heat input is a crucial factor that affects the welding deformation of thin plates. It influences the temperature field and distribution of thermal stress in the weld region, resulting in welding deformation [1]. By controlling the heat input reasonably, welding deformation can be reduced, and productivity improved. Therefore, researching the influence mechanism and control method of heat input is crucial in guaranteeing improved quality and efficiency in the thin plate welding process.

In addition, with the development of science and technology and the progress of industrial manufacturing, the requirements for high-quality, high-precision and high-reliability welding processes are getting higher and higher. Therefore, it is of great significance to promote the development of welding technology and industries to optimize the thin plate welding process and improve welding quality and reliability by studying the heat input control technology.

The effect of heat input on the deformation of thin plate welding is a popular research direction, and there are more related research results at home and abroad. Overseas, Okano S and other scholars at Osaka University, Japan, measured the temperature profile and distortion behavior of the welded plate during the welding process, and accurately simulated the thermo-mechanical behavior of the plate during the welding process by

using large deformation thermo-elastic-plastic analysis based on the modeling of the physical heat source of the arc. A comparison of the calculated and measured temperature profiles and deformation behavior verified the effectiveness of the developed numerical analysis technique [2]. Huang H and other scholars in the United States used an accurate hybrid iterative substructure and adaptive mesh method for the transient thermodynamic simulation of the laser welding process of a stainless steel sheet. The residual stress prediction was improved by considering various thermal effects in the numerical model, and the effects of laser welding heat input on the residual stress and weld distortion of stainless steel sheet were experimentally and simulatively investigated [3]. Amraei M. and other researchers in Australia studied the performance of butt-welded S700, S960, and S1100 steel thin plates at various heat input (HI) levels. A fully automated welding process was used to achieve high-quality and uniform welds. The butt welds were subjected to standard tensile tests and microhardness measurements. The microstructure of the heat affected zone (HAZ) of the welds was examined using scanning electron microscopy (SEM) [4]. Scientists, such as Eda S. of Osaka University, Japan, modeled the spot welding process in two dimensions, setting the pseudo arc as the current conductor between the wire and the base material; the heat input to the arc plasma was given via a simplified heat input model, and the effect of the gap between the thin plates was studied numerically [5]. Gadagi A et al. from India investigated the effect on the TMT stress required to reduce out-of-plane distortion using finite element simulation. In order to validate the thermo-mechanical model used in the finite element analysis (FEA), experiments were carried out considering on-board weld channels. The numerical simulation and test results were in good agreement. The effect of heat input rate on TMT in a reinforced plate was then investigated using the validated FEA model [6]. Scientists, such as Baruah M from India, have studied the micro-welding of 6 μm thin plate Ti4Al500V alloy butt joint configurations by developing a three-dimensional finite element model to simulate the temperature distribution of the joints and weld-induced distortion. The sequentially coupled thermo-mechanical model predicted the distortion using large displacement theory [7]. Sun J et al. systematically investigated the boundary position of the heat-affected zone of a thin plate only via the arc efficiency and the width of the heat source by combining numerical analysis and experimental ideas. In addition, the variation in the arc efficiency has a significant effect on the welding residual stress and deformation, while the reasonable variation in the heat source geometry parameters has less of an effect on the welding residual stress and deformation [8]. Perret W et al. used both analytical and numerical methods to calculate the temperature field due to welding thermal effects, and an analytical simulation of the temperature field distribution can be used instead of a numerical simulation for a transient thin plate that varies with cooling time [9].

Domestic research on thin plate welding also has a certain basis and has achieved great research results. Jiang Wenchang, from the China University of Petroleum, and other scholars used the finite element method to estimate the residual stress and deformation in the stainless steel composite plate repair weld, and studied the heat input and the number of welded layers on the residual stress and deformation of the impact [10]. In Shanghai Jiao Tong University, Li Zhiqiang and other scholars carried out the thermoelastic plastic finite element prediction of the welding deformation of a large thin plate welding structure, and then, through numerical analysis, studied the heat input, welding process and constraints on the thin plate welding deformation [11]. Lou Ming and colleagues from Shanghai Jiaotong University established a shell-cell-based sequential thermal structure finite element simulation method to predict the surface distortion induced during laser brazing. They experimentally validated their program through temperature and distortion measurements in the laser brazing of two 0.65 mm thick L-shaped steel plates [12]. Based on the experimental visualization of arc behavior, J. Chen et al. propose deriving adaptive planar and volumetric heat source models for different welding methods. They also calculate the effect of torch angle on temperature distribution and weld geometry [13]. Xu and colleagues utilized a biconical combined heat source model to simulate the transient

distribution of the temperature field. The simulation results demonstrate that the weld geometry aligns well with the experimental results, exhibiting a maximum prediction error of 5.84% [14]. Long et al. performed numerical simulations on butt joints with various thicknesses of bent plates at different welding speeds and discovered that both welding speed and bent plate thickness have a significant impact on the external deformation of the weld surface [15]. Guo et al. investigated the deformation and microstructure of welded joints made from metal plates and analyzed the post-welding hardness of those plates [16]. Teng utilized the birth–death cell technique to model the filling issue of fillet welds in metallic T-plate components and examined the impacts of boundary conditions and weld penetration on residual deformation after welding [17]. W. Liang and colleagues examined the welding deformation of thin plates made of aluminum alloy through both experimental and TEP finite element method. The predicted out-of-face deformation by the finite element method was consistent with the measured data [18]. J. Wang and colleagues proposed a finite element calculation approach utilizing the iterative substructure method and open multiprocessing parallel computation. This method predicts out-of-face weld deformation during the production of beveled welded structures with rectangular steel pipes. Additionally, it optimizes the clamping constraints and welding sequences to mitigate the aforementioned deformation [19]. H. Zhao and colleagues utilized thermoelastic–plastic finite element analysis to model the inherent deformation of welded joints in fillet-welded cantilever beam structures. This approach guarantees the precision of such structures [20]. H. Zhao and colleagues utilized thermoelastic–plastic finite element analysis to model the inherent deformation of welded joints in fillet-welded cantilever beam structures. This approach guarantees the precision of such structures [21]. The challenge of thin-walled pipe welding deformation is prominent, as outlined by Liu et al. Numerical simulations and experimental verification were utilized to investigate the effect of external constraints on the thin-walled pipe welding deformation of 304. The research shows that the most effective approach to alleviating the deformation is by reducing the constraint distance [22]. Lang and colleagues conducted research on the impact of various laser powers and welding speeds on the deformation of welded joints. The results indicated that higher welding temperatures resulted in greater welding depth [23]. El-Sayed et al. proposed that multi-pass friction stir processing can effectively solve the problem of premature onion cracking by accumulating higher strains to fully recrystallize the initial grains and improve the microstructure. Increasing the tool rotational speed increases the heat input and increases the grain size of the metal alloy, while improving the crushing effect of the rotation for a more uniform distribution of nanoparticles [24].

Thin bending plate welded structures are widely used in the aerospace, automotive, and other industrial fields. However, the uneven temperature distribution of the welding process generates welding stress and unpredictable welding deformation. It is important to consider these factors in the design and production of such structures. The residual deformation resulting from welding can seriously affect the dimensional accuracy and load-bearing properties of thin plate weldments. The primary types of welding deformation include shrinkage deformation, bending deformation, angular deformation, twisting deformation, wave deformation, and others. Heat input impacts both the deformation and type of deformation that occurs in thin bending plates. The impact of heat input on the thin bending plate, particularly the weld area, is a pressing issue both domestically and internationally. Successfully managing and controlling welding deformity in thin-walled components necessitates addressing this matter.

The ANSYS version 18.0 software was utilized to conduct numerical calculations of a bending plate in this study. Additionally, various heat inputs were implemented to carry out corresponding tests on the plate, evaluating the effects on welding deformation and weld morphology through indicator measurements. The deformation cloud diagram yielded through the comprehensive welding field analysis provided insights on the impact of heat input on deformation. Ultimately, all deformations were analyzed and subjected to finite element calculations.

2. Bent Plate Modeling and Verification

2.1. Bent Plate Modeling

A Q235 thin bending plate of size 300 mm \times 300 mm \times 3 mm with a radius of 500 mm was selected for analysis, and the welding process was single-pass overlay welding. The thermoelastic–plastic finite-element-method-based ANSYS version 18.0 software was utilized for simulation and forecasting. Figure 1 displays the finite element model of the bend plate. The 8-node hexahedral cell, SOLID70, having a single temperature degree of freedom at each node, was employed near the weld and edges. There were three degrees of freedom for displacements in the x, y, and z directions. In the structural analysis of the SOLID45 cell body selection, the geometry of the SOLID45 and SOLID70 cell bodies was identical. The thin curved plate had a cell size of 3 mm \times 1 mm \times 1 mm, and the entire model consisted of 26,244 nodes and 15,000 cells. The heat source for welding was moved along the x-axis, and the outputs from each step of the transient thermal analysis were used as loads for the structural calculations. The load action time corresponded to the heat source action time in the thermal analysis. To avoid the rigid displacement of the model, a three-point constraint was applied as the boundary condition in the subsequent structural analysis, as shown in the figure.

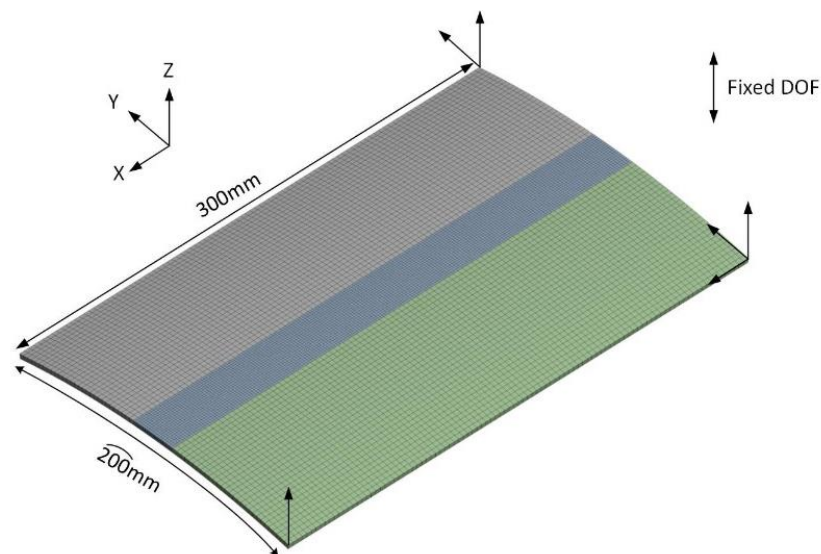


Figure 1. Finite element model and constraints of bending plate.

2.2. Experimental Validation of Finite Element Models

In this article, a digital image correlation-based testing method was utilized to confirm the precision of the finite element model for a thin bending plate. Technical abbreviations such as DIC will be fully explained when first used. The writing employs a clear and objective language without filler words, colloquialisms, or figurative language. Figure 2 displays the schematic diagram of the welding test setup and the test setup test diagram. A formal register and grammatical correctness are maintained, and the text adheres to a conventional academic structure. The 3D digital image correlation measurement (DIC) setup comprised two cameras (model Aca1600-20 gm, resolution 1626 \times 1236 pix, pixel size 4.4 μ m \times 4.4 μ m \times width 400 mm \times 300 mm), a control system, a post-processing system, and an auxiliary device. The camera acquired dynamic deformation images, the control system managed hardware operation, and the post-processing system calculated the deformation displacement and strain.

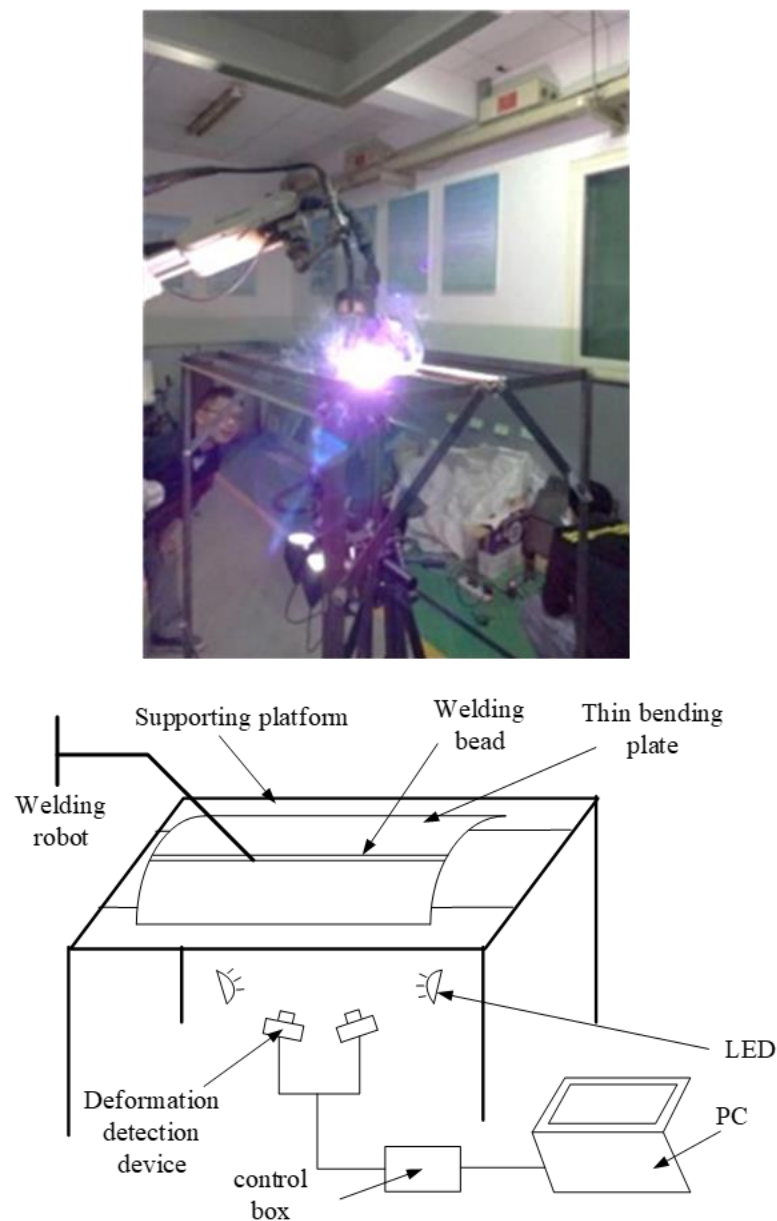


Figure 2. Welding test equipment experimental bench and schematic diagram.

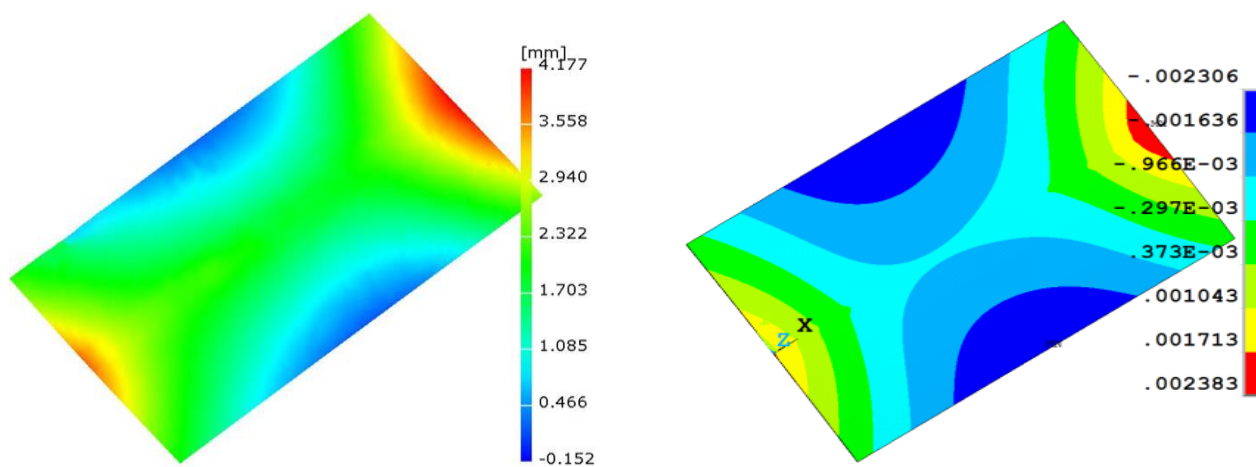
Before conducting the deformation detection test, it was essential to grind off the oxide layer on the thin bending plate's surface and cleanse any surface debris using acetone. The temperature in the weld area tended to be higher. To prepare for the scattering of the spot, we conducted a deformation detection test on the surface of the weld and the surrounding area of the C-3 adhesive (which has a heat-resistant temperature of 1460 °F and a coefficient of linear expansion of $12.9 \times 10^{-6}/^{\circ}\text{C}$). Finally, we coated the scattering spot on the other detection area with high-temperature paint.

To prevent the arc light of TIG welding from affecting the captured image, the welding torch traveled above the bending plate while the DIC equipment captured the image from below. During welding, a horizontal placement of the bending plate on the welding table was necessary. The welding robot's arm was perpendicular to the welding surface to control the torch's starting and stopping positions and paths. Additionally, a calibrated camera was placed directly below the bending plate. The welding process required the adjustment of the camera group and thin plate position to ensure the complete capture of the welded thin plate. Additionally, camera acquisition parameters and light source adjustments were necessary for the uniform brightness of the welded thin plate. During the

welding process, the DIC captured two pictures per second in order to maintain consistency with the welding start time, as the bending plate underwent large deformations. During the cooling process, one picture per second was collected. Once the welding was complete, the plate was allowed to cool for 10–15 min before ceasing photo acquisition.

The data were processed in the DIC computing system, and a scattering field covered the entire bending plate as much as possible. For this experiment, a sub-area size of 30 pixels \times 30 pixels with a step size of 15 pixels \times 15 pixels was selected. Next, a seed point was chosen on each side of the weld within the scattering field, ensuring they were in the same position in both the left and right cameras. After selecting the seed points, all scattering spots within the scattering domain were automatically matched to complete the matching process. The first image was used as a reference for calculating and extracting the desired test results.

The reliability of the structural calculations was confirmed through a comparison of the computed results of the welding deformation of the thin plate with the actual measurements. Figure 3 exhibits the out-of-plane deformation cloud diagram of the DIC measurement, as well as the numerical simulation following the complete cooling down of the bending plate. Since the welding table obstructs the bending plate's edge by approximately 16 mm during testing, the calculated outcomes were assumed to be identical to those of the test measurement. As shown in the figure, both the experimental and calculated results indicate that the bending plate underwent saddle deformation upon cooling and welding. The maximum deformation observed in the experiment was 10.85 mm, while the maximum deformation obtained through finite element analysis was 9.96 mm. The discrepancy between the calculated and experimental results was approximately 8%, which is within an acceptable range.



(1) Experimental test deformation results (2) Finite element prediction deformation results

Figure 3. Cloud view of external deformation after the complete cooling of the bending plate.

2.3. Deformation Detection Displacement Calculation Method

Three-dimensional digital image correlation detection technology mainly includes image correlation technology and stereo vision technology, in which image correlation technology can obtain the full-field dynamic deformation data, while stereo vision technology can obtain three-dimensional information on the deformed object.

The calculation of deformation displacement is depicted in Figure 4, where the two-dimensional scattering correlation method is referred to as DIC-A and the binocular stereo matching method is labeled DIC-B. The deformation state of the measured object from the left camera is shown in Image 1-n. Similarly, the deformation state of the measured object from the right camera is displayed in Image 2-n, where n represents the nth state of the object being measured. “Images 1-1 and 1-2 depict the recordings from two cameras capturing the object in its initial state. The images in state 2, where the object has been

deformed, are represented by Images 1-2 and 2-2, respectively. Subsequent images follow this numbering convention." In "Image 1-1," due to the welding's high temperature and the bright light's influence, the captured images require additional correction to obtain a clear "Image 1-1." Likewise, all acquired images from the left and right cameras need to undergo correction to ensure clarity.

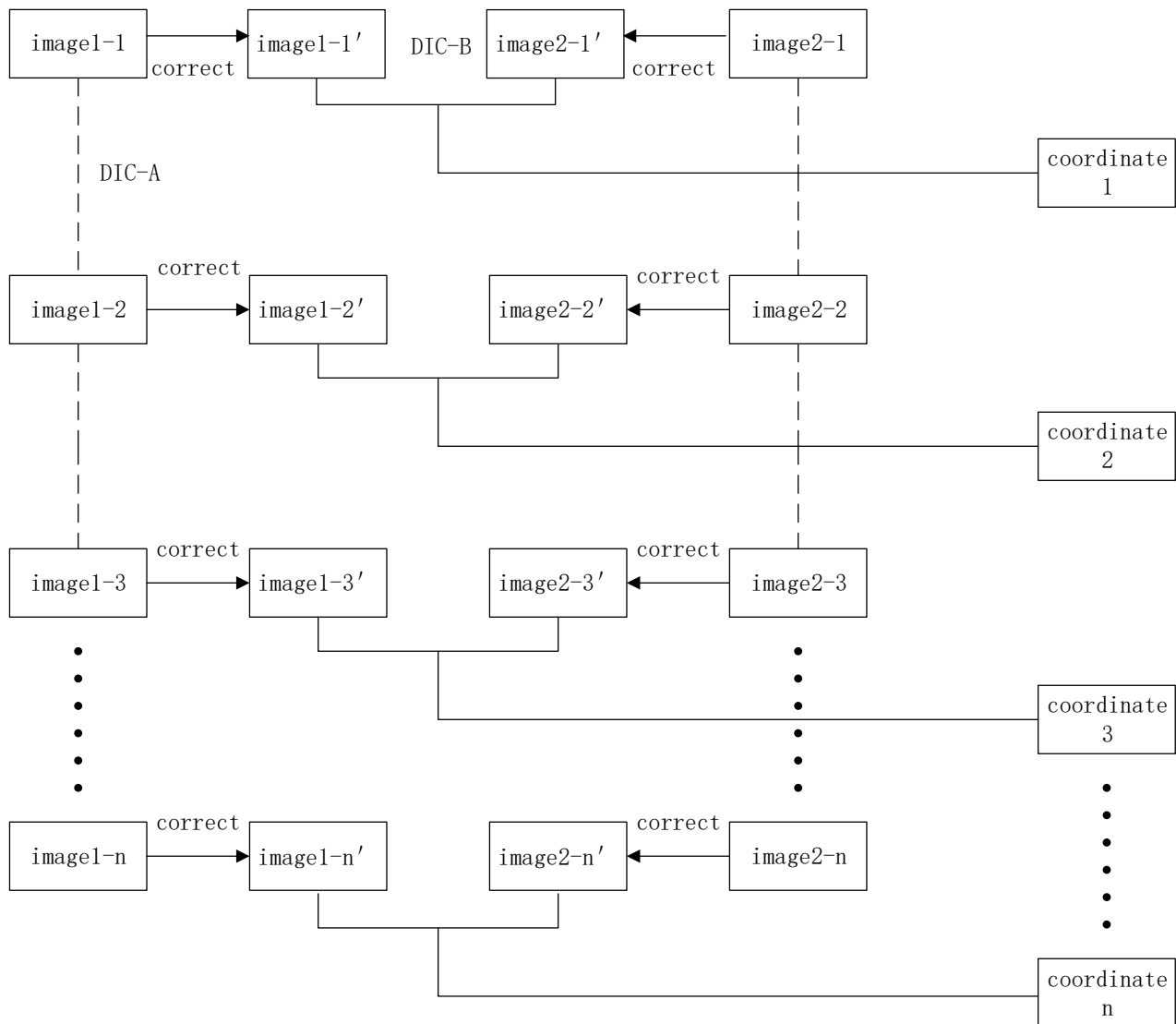


Figure 4. Displacement calculation flowchart.

In "Image 1-1", the analysis selects the calculation region, which is then divided into related regions. The first related region's corresponding center pixel point is denoted, resulting in a point set. The binocular stereo matching method is utilized to compute stereo matching and 3D reconstruction for "Image 1-1'" and "Image 2-1'". The corresponding spatial coordinates of the points are obtained as Coordinate 1. To obtain spatial coordinates corresponding to the points in "Image 1-1'" and "Image 1-2'", the 2D scattering correlation method is employed to correlate "Image 1-1'" and "Image 1-2'". The two-dimensional scattering correlation method calculates the correlation between "Image 1-1'" and "Image 1-2'", yielding the corresponding point sets, denoted by $P' = \{(x'_i, y'_i), i = 1, \dots, n\}$. Subsequently, the binocular stereo matching method is employed to determine the stereo matching between "Image 2-1'" and "Image 2-2'", and the resulting three-dimensional reconstruction produces the state of "Image 2-2'". Technical abbreviations are clarified upon first usage. Objective, formal language is utilized with precise, subject-specific termi-

nology. The text follows conventional academic structures and citation styles, and adheres to correct grammar and spelling. Three-dimensional reconstruction is utilized to obtain the spatial coordinates of the points in state 2, referred to as “coordinate 2.” The displacement to be calculated is the difference between “Coordinate 1” and “Coordinate 2.” By repeating this process, displacement data are obtained for each deformation state in the entire deformation process.

3. Effect of Heat Input on Welding Distortion of Thin Bending Plates

3.1. Full-Field Deformation Analysis of Thin Curved Plates

Welding heat input has a greater impact on welding deformation. In order to study the effect of welding deformation on a thin bending plate under different heat inputs, when the heat input is 173–435 J/mm, we analyzed the internal deformation law outside the face of the thin bending plate.

Table 1 shows five groups of welding processes with different heat inputs, the radius of the bending plate is 500 mm for all of them, and the material is mild steel Q235. The heat input is calculated using the following formula:

$$Q_{net} = \frac{\eta UI}{v} \quad (1)$$

where η is the thermal efficiency, U is the welding voltage, I is the welding current, and v is the welding speed.

Table 1. Thermal input parameters.

Bend Plate Size mm × mm × mm	Weld Current I/A	Weld Voltage U/V	Thermal Efficiency η	Heat Input J/mm	Weld Speed mm/s
300 × 200 × 3	90	12	0.8	173	5
300 × 200 × 3	110	13.5	0.8	238	5
300 × 200 × 3	130	14.5	0.8	302	5
300 × 200 × 3	150	15	0.8	360	5
300 × 200 × 3	170	16	0.8	435	5

Figure 5 shows the full-field deformation cloud diagram of the bending plate after welding and cooling under different heat inputs, it can be seen that the bending plate in this heat input range of out-of-face deformation is saddle-shaped; with the increase in heat input, the maximum positive out-of-face deformation and maximum negative out-of-face deformation of the bending plate increase accordingly, in which the maximum positive out-of-face deformation increased from 0.383 mm to 2.511 mm, and the maximum negative out-of-face deformation increased from 1.095 mm to 2.467 mm. With an increase to 2.467 mm, the maximum positive outward deformation sees a relatively large increase, indicating that the heat input on the longitudinal surface deformation of the curved plate is relatively large, which is mainly due to the initial curvature of the curved plate in the transverse direction of the formation of larger constraints.

The relationship between the maximum out-of-plane deformation of the bent plate and the heat input is shown in Figure 6, where the heat input shows an increasing relationship with the maximum out-of-plane deformation, and the maximum out-of-plane deformation of the bent plate is fitted linearly:

$$\delta_{\max} = 0.013Q_{net} - 0.65 = 0.013(Q_{net} - 50) \quad (2)$$

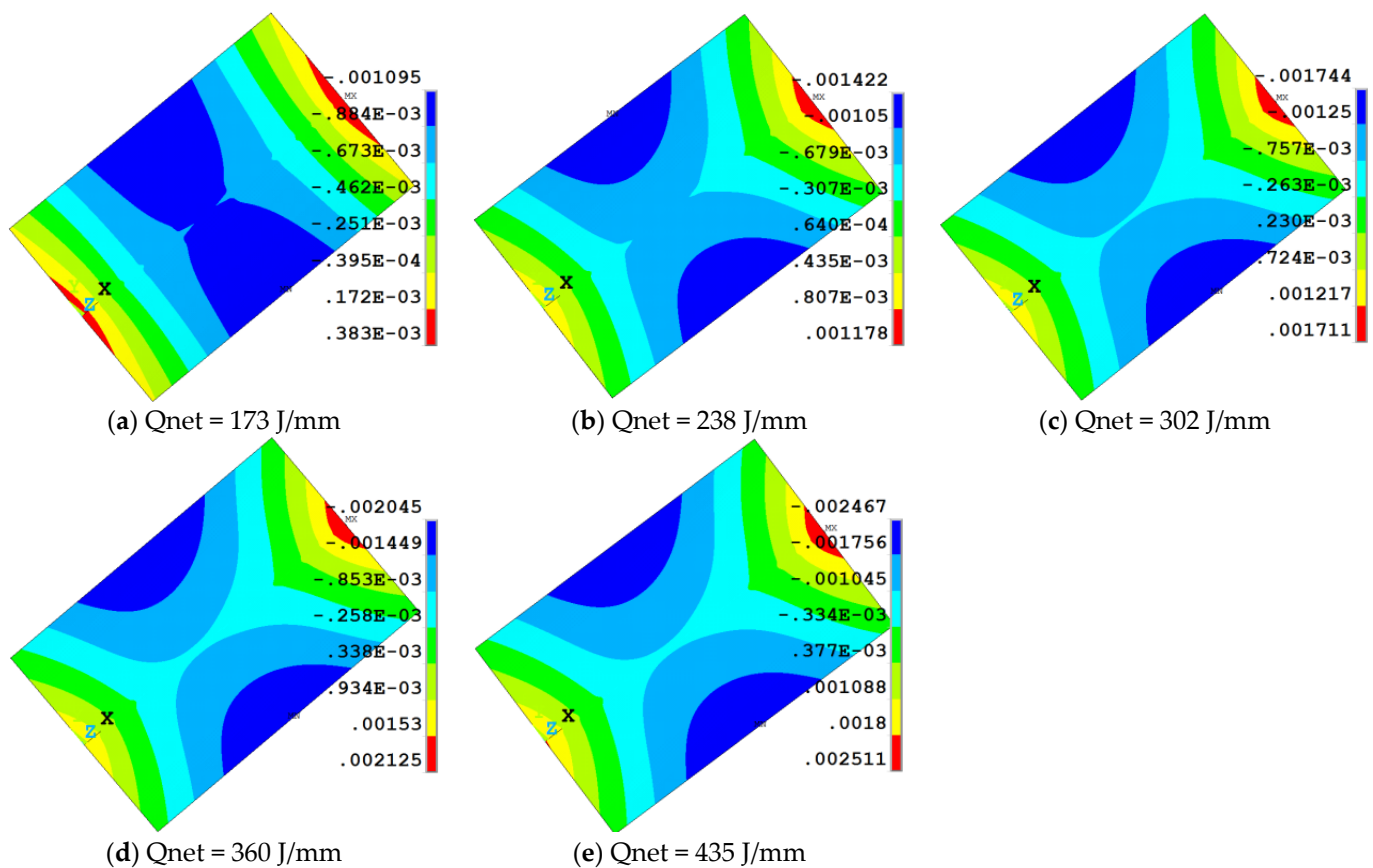


Figure 5. Out-of-plane deformation of bent plate with different heat inputs.

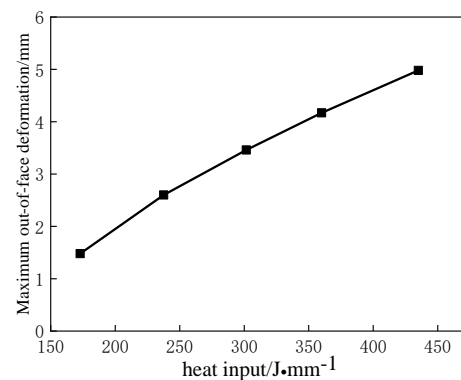


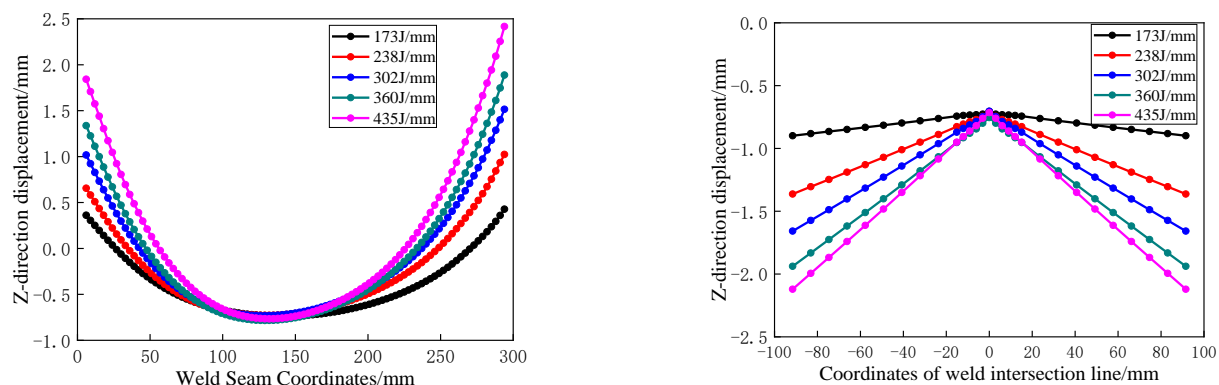
Figure 6. Maximum out-of-plane deformation vs. heat input.

From the above fitting equation, it can be seen that the heat input needs to reach a certain threshold value before the bending plate will deform out of the face, and this parameter is of great significance in welding engineering.

3.2. Analysis of out-of-Face Deformation of Thin Curved Plate

Figure 7 shows the out-of-plane deformation of the bending plate truncation line 1 (shown in Figure 2) and truncation line 2 (shown in Figure 2) under different heat inputs. Figure 7a, the truncation line 1 along the weld direction of the bending plate under different heat inputs shows concave deformation, and the z-direction displacement at the center of the bending plate is approximately the same, while the z-direction deformation of the two ends of the weld increases with the increase in the heat inputs, and the degree of the bending is more obvious, which shows that the heat inputs have greater influence on the deformation of the two ends of the weld in the longitudinal direction. The influence of

heat input on the deformation of the two ends of the weld in the longitudinal direction is larger. Figure 7b, the bending plate in the transverse direction has a downward angular deformation; with the increase in heat input, the transverse surface angular deformation also increases. Thus, it can be seen that the bent plate is a saddle-shaped deformation formed by the combination of the upper parabola and the lower triangle, and; with the change in heat input, the deformation at the lowest point of the longitudinal parabola and the deformation at the highest point of the transversal triangle are unchanged. This is due to the fact that, with the increase in heat input, the longitudinal shrinkage and transverse shrinkage increase, the increase in internal stress leads to an increase in deformation, and at the same time, in order to coordinate the deformation, the transverse and longitudinal directions appear to be deformed in the opposite direction, respectively.



(a) Out-of-plane deformation of truncation line 1 (b) Out-of-plane deformation of truncation line 2

Figure 7. Out-of-plane deformation of different heat input bending plates.

3.3. Analysis of in-Face Deformation of Thin Curved Plate

The distribution of longitudinal/transverse strains at the center of the weld of the bent plate under different heat inputs is shown in Figure 8. From the relationship between the longitudinal plastic strain of the weld and the heat input (Figure 8a), it can be seen that the heat input on the longitudinal strain edge effect of the bending plate weld is very obvious; with the increase in heat input, the longitudinal strain in the fluctuating region at both ends of the weld increases, and the effect on the weld start position is more obvious. In the middle of the stable region (50–250 mm), with the increase in heat input, the longitudinal strain also corresponds to a slow increase in the overall heat input on the weld position in the middle of the smaller. As can be seen from the Figure 8b, the whole transverse plastic strain of the weld increases with the increase in heat input, and the boundary effect also only affects the weld within 50 mm at both ends of the weld, and the transverse plastic strain at the boundary gradually increases until it stabilizes. In the stabilized zone of transverse strain, the effect of heat input on weld strain is mainly due to the increase in heat input, which leads to the increase in weld contraction force and the corresponding increase in transverse strain. Therefore, the heat input has a greater effect on the transverse plastic strain of the weld and a smaller effect on the longitudinal plastic strain. At the same time, the heat input only affects the magnitude of the value of the weld strain, and does not affect the scope and trend of the edge effect.

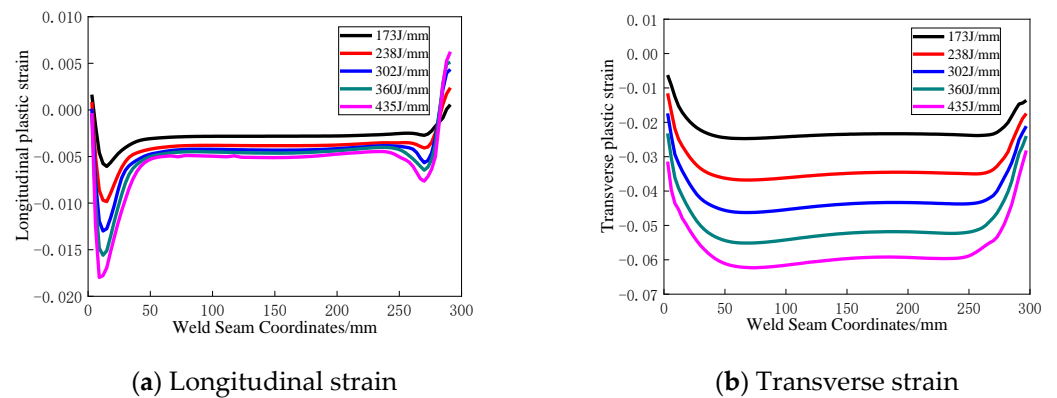


Figure 8. Strain distribution of welds in bending plates with different heat inputs.

Figure 9 shows the relationship between longitudinal/transverse shrinkage and heat input at the weld seam of a thin bending plate, and it can be seen that both the total longitudinal shrinkage and the total transverse shrinkage of the bending plate increase linearly with the increase in the heat input, and the relationship curve between the in-plane shrinkage of the bending plate and the heat input is fitted linearly:

$$\delta_L = 6.7 \times 10^{-4} Q_{net} - 0.11 \quad (3)$$

$$\delta_T = 9.4 \times 10^{-4} Q_{net} - 0.022 \quad (4)$$

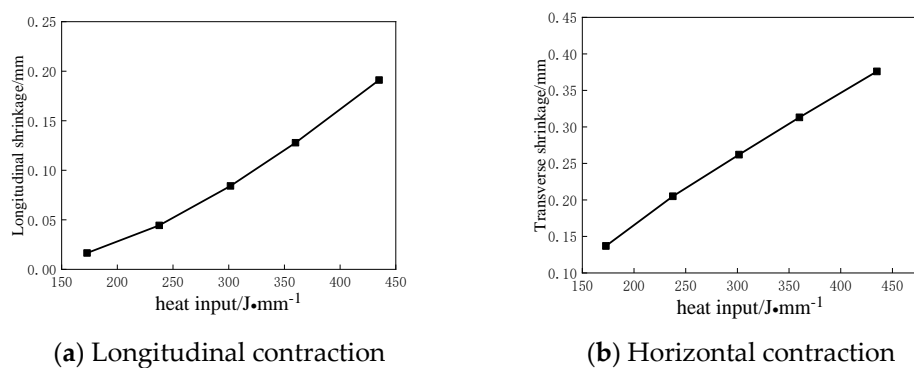


Figure 9. In-plane shrinkage for different heat input bending plates.

In the formula, δ_L is the longitudinal shrinkage, δ_T is the transverse shrinkage, and Q_{net} is the welding heat input.

From the above two fitting equations, it can be seen that the effect of heat input on transverse shrinkage is relatively large, but due to the transverse curvature constraints, the transverse out-of-plane deformation of the curved plate is not as pronounced as the longitudinal out-of-plane deformation.

Through the above finite element calculation of the welding deformation of the bent plate under different heat input, it can be seen that the heat input on the surface of the bent plate outside the deformation and the surface deformation have a certain effect, so in the development of the welding process parameters of the bent plate, under the premise of meeting the performance of the weldments, it is appropriate to choose the appropriate heat input process parameters.

4. Conclusions

In this paper, the thermoelastic plastic finite element method is used to study the effect of welding heat input on the deformation of a thin bending plate. The accuracy of the finite element model is verified using a non-contact inspection test based on the digital image

correlation method. The deformation law of a thin bending plate is obtained by studying the deformation of the whole welding field and weld zone of the bending plate under different heat inputs (173–435 J/mm). The following main research results were obtained:

- (1) In the heat input range, the thin bending plate deformation is consistent, the residual deformation has a longitudinal parabolic transverse lower triangular saddle shape, and the maximum out-of-face deformation and heat input have a positive linear relationship.
- (2) The heat input on the weld transverse shrinkage is relatively large, but due to the role of the transverse curvature constraints of the thin bending plate, the bending plate transverse out-of-plane deformation is not as obvious as the longitudinal out-of-plane deformation. The bent plate weld area of the longitudinal and transverse shrinkage increases with the increase in heat input; the edge effect only affects the weld area at both ends of the shrinkage of 50 mm.
- (3) The longitudinal/transverse shrinkage of the weld zone of the thin bending plate and the heat input show a certain linear relationship, the empirical formula of which is of great significance in welding engineering.

Author Contributions: Conceptualization, N.G.; methodology, N.G. and H.H.; software, X.T.; validation, N.G. and X.T.; investigation, X.M.; resources, X.W.; data curation, N.G.; writing—original draft preparation, X.T.; writing—review and editing, H.H.; supervision, X.M.; project administration, X.W.; funding acquisition, N.G. All authors have read and agreed to the published version of the manuscript.

Funding: This research was funded by the Natural Science Foundation of Henan Province of China (Grant No. 232300421336); the National Key R&D Program of China (Grant No. 2021YFB2011000); and the Wind Tunnel Industry Project of Longmen Laboratory (Grant No. LMFICY2023001).

Informed Consent Statement: Informed consent was obtained from all subjects involved in the study.

Data Availability Statement: Data are contained within the article.

Conflicts of Interest: The authors declare no conflict of interest.

References

1. Wu, C.; Kim, J.-W. Numerical prediction of deformation in thin-plate welded joints using equivalent thermal strain method. *Thin-Walled Struct.* **2020**, *157*, 107033. [\[CrossRef\]](#)
2. Okano, S.; Mochizuki, M. Transient distortion behavior during TIG welding of thin steel plate. *J. Mater. Process. Technol.* **2017**, *241*, 103–111. [\[CrossRef\]](#)
3. Huang, H.; Tsutsumi, S.; Wang, J.; Li, L.; Murakawa, H. High performance computation of residual stress and distortion in laser welded 301L stainless sheets. *Finite Elem. Anal. Des.* **2017**, *135*, 1–10. [\[CrossRef\]](#)
4. Amraei, M.; Ahola, A.; Afkhami, S.; Björk, T.; Heidarpour, A.; Zhao, X.-L. Effects of heat input on the mechanical properties of butt-welded high and ultra-high strength steels. *Eng. Struct.* **2019**, *198*, 109460. [\[CrossRef\]](#)
5. Eda, S.; Ogino, Y.; Asai, S.; Hirata, Y. Numerical study of the influence of gap between plates on weld pool formation in arc spot welding process. *Weld. World* **2018**, *62*, 1021–1030. [\[CrossRef\]](#)
6. Gadagi, A.; Mandal, N.R.; Podder, D. Effect of Rate of Heat Input on Thermomechanical Tensioning for Distortion Mitigation. *J. Ship Prod. Des.* **2019**, *35*, 103–114. [\[CrossRef\]](#)
7. Baruah, M.; Bag, S. Influence of heat input in microwelding of titanium alloy by micro plasma arc. *J. Mater. Process. Technol.* **2016**, *231*, 100–112. [\[CrossRef\]](#)
8. Sun, J.; Klassen, J.; Nitschke-Pagel, T.; Dilger, K. Effects of heat source geometric parameters and arc efficiency on welding temperature field, residual stress, and distortion in thin-plate full penetration welds. *Int. J. Adv. Manuf. Technol.* **2018**, *99*, 497–515. [\[CrossRef\]](#)
9. Perret, W.; Schwenk, C.; Rethmeier, M. Comparison of analytical and numerical welding temperature field calculation. *Comput. Mater. Sci.* **2010**, *47*, 1005–1015. [\[CrossRef\]](#)
10. Jiang, W.C.; Wang, B.Y.; Gong, J.M.; Tu, S.T. Finite element analysis of the effect of welding heat input and layer number on residual stress in repair welds for a stainless steel clad plate. *Mater. Des.* **2011**, *32*, 2851–2857. [\[CrossRef\]](#)
11. Li, Z.; Feng, G.; Deng, D.; Luo, Y. Investigating Welding Distortion of Thin-Plate Stiffened Panel Steel Structures by Means of Thermal Elastic Plastic Finite Element Method. *J. Mater. Eng. Perform.* **2021**, *30*, 3677–3690. [\[CrossRef\]](#)
12. Lou, M.; Cai, W.; Huang, J.; Wang, H.-P.; Li, Y.; Carlson, B.E.; Poss, M.G. Simulation of laser brazing of sheet panels and parametric studies of thermally-induced distortion reduction. *J. Manuf. Process.* **2020**, *60*, 1–10. [\[CrossRef\]](#)

13. Chen, J.; Wu, C.S.; Chen, M.A. Improvement of welding heat source models for GTAW-MIG hybrid welding process. *J. Manuf. Process.* **2014**, *16*, 485–493. [[CrossRef](#)]
14. Xu, J.; Chen, C.; Lei, T.; Wang, W.; Rong, Y. Inhomogeneous thermal-mechanical analysis of 316L butt joint in laser welding. *Opt. Laser Technol.* **2019**, *115*, 71–80. [[CrossRef](#)]
15. Long, H.; Gery, D.; Carlier, A.; Maropoulos, P.G. Prediction of welding distribution in butt joint of thin plates. *Mater. Des.* **2009**, *30*, 4126–4135. [[CrossRef](#)]
16. Guo, H.; Hu, J.; Tsai, H.L. Three-Dimensional Modeling of Gas Metal Arc Welding of Aluminum Alloys. *J. Manuf. Sci. Eng.* **2010**, *132*, 021011. [[CrossRef](#)]
17. Teng, T.L.; Le, T.K.; Ngo, V.L. Injury analysis of pedestrians in collisions using the pedestrian deformable model. *Int. J. Automot. Technol.* **2010**, *11*, 187–195. [[CrossRef](#)]
18. Liang, W.; Murakawa, H.; Deng, D. Estimating inherent deformation in thin-plate Al-alloy joint by means of inverse analysis with the help of cutting technique. *Adv. Eng. Softw.* **2016**, *99*, 89–99. [[CrossRef](#)]
19. Wang, J.; Yi, B. Effective thermal elastic plastic finite element computation for welding distortion investigation of pozidriv-type welded structure with rectangular pipes and its mitigation. *Proc. Inst. Mech. Eng. Part B J. Eng. Manuf.* **2020**, *234*, 1729–1741. [[CrossRef](#)]
20. Zhao, H.; Zhang, Q.; Niu, Y.; Du, S.; Lu, J.; Zhang, H.; Wang, J. Influence of triangle reinforcement plate stiffeners on welding distortion mitigation of fillet welded structure for lightweight fabrication. *Ocean Eng.* **2020**, *213*, 107650. [[CrossRef](#)]
21. Huang, T.D.; Harbison, M.; Kvidahl, L.; Niolet, D.; Walks, J.; Stefanick, K.; Phillippi, M.; Dong, P.; DeCan, L.; Caccese, V.; et al. Reduction of Overwelding and Distortion for Naval Surface Combatants, Part 1: Optimized Weld Sizing for Lightweight Ship Structures. *J. Ship Prod. Des.* **2014**, *30*, 184–193. [[CrossRef](#)]
22. Liu, Y.; Wang, P.; Fang, H.; Ma, N. Mitigation of residual stress and deformation induced by TIG welding in thin-walled pipes through external constraint. *J. Mater. Res. Technol.* **2021**, *15*, 4636–4651. [[CrossRef](#)]
23. Lang, Q.; Zhang, X.; Song, G.; Liu, L. Effects of different laser power and welding speed on the microstructure and mechanical properties of TRIP joints in laser-TIG arc hybrid lap filler wire welding. *Mater. Today Commun.* **2021**, *29*, 102925. [[CrossRef](#)]
24. El-Sayed, M.M.; Shash, A.; Abd-Rabou, M.; ElSherbiny, M.G. Welding and processing of metallic materials by using friction stir technique: A review. *J. Adv. Join. Process.* **2021**, *3*, 100059. [[CrossRef](#)]

Disclaimer/Publisher's Note: The statements, opinions and data contained in all publications are solely those of the individual author(s) and contributor(s) and not of MDPI and/or the editor(s). MDPI and/or the editor(s) disclaim responsibility for any injury to people or property resulting from any ideas, methods, instructions or products referred to in the content.